



Investigation of an Innovative Technique for R.C. Piles Reinforced by Geo-Synthetics Under Axial Load

Mona I. Badawi¹, Mahmoud Awwad^{1*}, Mohab Roshdy¹, El-Sayed A. El-Kasaby¹

¹ Department of Civil Engineering, Benha Faculty of Engineering, Benha University, Benha, Egypt.

Received 06 June 2024; Revised 11 September 2024; Accepted 17 September 2024; Published 01 October 2024

Abstract

The use of alternative reinforcement material to enhance the performance of the pile capacity has gained increasing interest in recent years. This study seeks to probe the improvement of the ultimate pile capacity, reduction the deformation, and the financial results of using alternative reinforcement material such as glass fiber-reinforced polymers (GFRP), geosynthetics geogrids, as well as a combination of geosynthetics geogrids and a central steel bar. Axial load investigations were conducted on circular piles with 150 mm diameter and 1050 mm height. The experimental results revealed an improvement in the axial capacity of up to 25.4% and an enhancement in performance represented in ductility. Furthermore, financial and weight comparisons showed a decrease in the cost by up to 15%. Moreover, a nonlinear finite element (FE) study with Abaqus software was employed to standardize the numerical outcomes with the laboratory findings. The FE analysis was also verified with the previous studies. The 3D nonlinear finite element numerical model performed showed convergence with and without representing the surrounding soil of the pile; thus, confirming the adequacy of the experimental setup adopted. Finally, a suggested theoretical equation is developed to evaluate the change in pile axial load capacity based on the use of different reinforcement materials. The application of the proposed theoretical equation provides further insight into the governing equation involving different reinforcing materials.

Keywords: Geosynthetics Geogrids; GFRP; Piles; Axial Load; FEM.

1. Introduction

Pile foundation construction has included the employment of conventional materials like steel, timber, and concrete. However, yonder many issues lie the utilization of these materials, particularly when cast in corrosive, harsh environments and overall life cycle cost [1, 2]. Mitigation of steel corrosion in deep foundations requires full replacement of the existing piles, which represents the paramount problem in the construction cost [3]. Over the years, there has been considerable research seeking alternative materials to solve the issues pertaining to corrosion of steel and deterioration of deep concrete piles [4, 5]. Composite piles constructed using fiber-reinforced polymers (FRP) and geosynthetic geogrids (G) have been proposed as possible alternatives. The axial behavior and performance of FRP composite piles have been extensively examined experimentally [6-15]. The utilization of FRP proves beneficial owing to its efficient lightweight-to-strength ratio, exceptional durability, strong corrosion resistance, and adhesive strength, rendering it a practical and cost-effective choice. These advantages led to the rapid development of FRP across numerous industries, driving production costs to appealing levels [16]. Conventional FRP piles either use a high-density polyethylene matrix reinforced with steel or glass fiber-reinforced polymers (GFRP) in the configuration of hollow shells [17]. The driving response of composite piles is primarily a result of factors such as the specific type of driving hammers employed, soil

* Corresponding author: mahmoud.awad@bhit.bu.edu.eg

 <http://dx.doi.org/10.28991/CEJ-2024-010-10-011>



© 2024 by the authors. Licensee C.E.J, Tehran, Iran. This article is an open access article distributed under the terms and conditions of the Creative Commons Attribution (CC-BY) license (<http://creativecommons.org/licenses/by/4.0/>).

resistance, pile impedance, and the efficiency resistance of the pile materials. Although FRP piles present significant outcomes related to cost-effectiveness and structural capacity, their widespread adoption has been hindered by the scarcity of established guidelines and regulations, particularly concerning their installation procedures.

Pando et al. [18] investigated a large-scale pile to explore the response difference between driven piles constructed as a square pre-cast pre-stressed concrete pile (PSP), concrete-filled tubular FRP piles (CFTP), and steel-reinforced recycled plastic pile (SRRP). According to field test findings, within a spectrum of bending moments, the flexural stiffness diminishes in the sequence from the (PSP) to the (CFTP) to the (SRRP). In terms of axial stiffness, the pre-stressed concrete pile was like the FRP pile and approximately 2.5 times that of the recycled plastic pile. The lateral performance of the pre-stressed and FRP piles was similar. Zhang & Hadi [19] developed a new composite pile that combines geogrid-confined geopolymer concrete (GPGC) piles with fiber-reinforced polymer-polyvinyl chloride-confined concrete core (FPCC). This new composite pile showed improved ductility and sustained higher axial loads than those of GPGC piles without FPCC. The application of GFRP composite reinforcing bars for hollow concrete columns (HCCs) and the outcome of the ratio of their reinforcement on HCC structural response was examined by AlAjarmeh et al. [20]. Their results indicated that the increased ratio was inversely proportional to the ductility performance of the HCC. The findings indicated that, at an equivalent reinforcement ratio, smaller diameter bars exhibited a 12% higher level of confinement efficiency compared to larger diameter bars. GFRP bars inserted in HCC had a crushing strain that was 52.1% of the maximum tensile strain.

Pham et al. [21] studied the impact of utilizing the geotextile as encasing for gravel column (G-GC) on the peak capacity and deformation in soft clay soil (SCS). Test results revealed that the peak capacity of the SCS soil has been improved by using G-GC columns by 1.85 times the untreated soil. Moreover, the utilization of geosynthetic materials has been explored in improving the loose sand soil settlement of embankments by AlSirawan et al. [22, 23] and Alnmr & AlSirawan [24]. The presence of two geotextile layers plays a vital role in reducing the maximum settlement by up to 30%. In addition, Pham [25] conducted a numerical survey of the load transfer philosophy of Geosynthetic-reinforced and pile-supported (GRPS) embankments taking into consideration the soil embankment, pile, geosynthetics, and subsoil interaction. The findings revealed that these strategies differ in their capabilities for differential settlement and maximum capacity.

Based on the literature review, the availability of Triaxial Geosynthetics Geogrid (TX) in the global and local stores enabled the authors to engage in the study to develop a corrosion-resistant alternative to steel pile reinforcement. Furthermore, a lack of studies has converged on raising the axial capacity and reinforcement corrosion resistance of piles by using (TX) geogrids and is limited to evaluating only one type of reinforcement. This study strives to reduce this shortage by investigating the axial carrying capacity and the response of piles reinforced with different materials at a laboratory scale. The proposed investigation covers concrete piles reinforced with different materials like GFRP bars, geosynthetics geogrids with a middle core of steel bar. The materials used in the reinforcement are referred to throughout this manuscript using the abbreviations code as follows: Steel (S), GFRP bars (L), Geosynthetics geogrids TX130 (GA), Geosynthetics geogrids TX150 (GB). The experimental results are then numerically validated through the finite element (FE) modeling specialized software program, Abaqus/CAE Standard. This model enables the modeling of the RC piles in three-dimensional space while taking into consideration the material nonlinearity of concrete in addition to the elastic response of the FRP bars and geosynthetics. The economic feasibility of the reinforcement concerning the enhancement in the axial capacity is also analyzed.

2. Research Methodology

This study was conducted in three phases as follows: (i) experimentally investigation of mechanical properties of different materials (Steel, GFRP, and Geotextile geogrid) and performance of piles reinforced with the indicated materials, (ii) Conducting finite element models to represent and verify with the laboratory results, and (iii) Propose a formula to estimate the ultimate axial capacity of the innovative material – reinforced pile. Figure 1 shows the flowchart of this study framework.

2.1. Specimen Configurations and Test Matrix

A total of six piles reinforced with GFRP, steel, and Geotextile were cast, and laboratory examined. All piles have an external diameter of 150 mm and are 1050 mm in length. The ratio of reinforcement (A_s) to concrete (A_c) is kept approximately the same to provide a proper comparison. The tested specimen dimensions were selected to properly suit the laboratory conditions. It is mentioned that compression members have a height-to-diameter ratio equal to or greater than 3 as stated in the ACI 318M-11 [26]. The tested specimen's height-to-diameter ratio in this investigation was close to 7. Each group is compared to a reference reinforced concrete (RC pile), which is referred to as the control specimen

(PS). The first group consists of one pile specimen formed of four bars with an 8 mm diameter, namely PL, which is reinforced with GFRP. Additionally, and to eliminate any effect that could be introduced by the stirrup, a 6 mm diameter spiral stirrup formed of mild steel was used for the piles in this group. The second group consists of two pile specimens, namely PGA and PGB, which were reinforced with Geosynthetics geogrids TX130 (GA) and Geosynthetics geogrids TX150 (GB), respectively, formed as a cylindrical roll. The third group consists of two pile specimens, namely PSGA and PSGB, which were reinforced with Geosynthetics geogrids TX130 (GA) and Geosynthetics geogrids TX150 (GB), respectively, formed as a cylindrical roll with an additional 12 mm diameter steel bar in the middle of the core. Table 1 lists the reinforcement type and ratios of the study specimen.

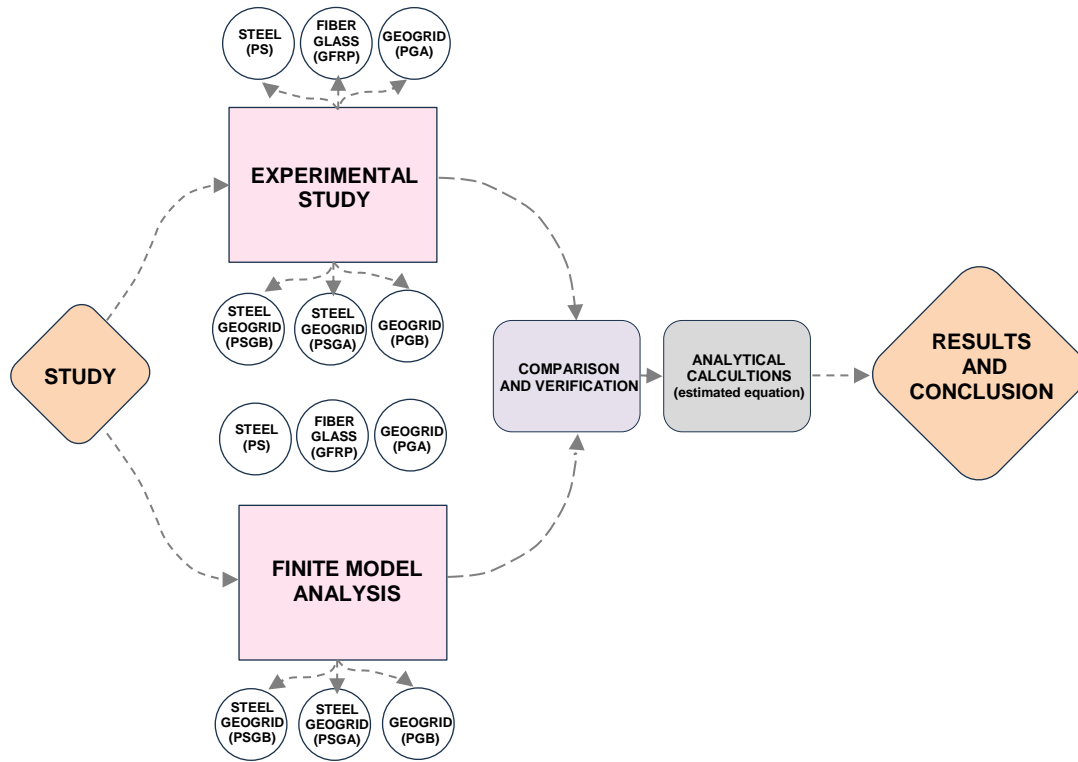


Figure 1. flowchart of the framework

Table 1. Experimental program indicating the piles within each of the three groups

Group	Reference		First	
Schematic				
Pile Code	PS		PL	
Reinforcement	Steel		GFRP bars	
Reinforcement ratio (AS / AC) %	1.13		1.13	
Schematic				
Pile Code	PGA	PGB	PSGA	PSGB
Reinforcement	Geogrid TX130	Geogrid TX150	Steel bar + Geogrid TX130	Steel bar + Geogrid TX150
Reinforcement ratio (AS / AC) %	1.13	1.15	1.13+0.64	1.15+0.64

2.2. Material Properties

The design mix for the concrete is constant for all the test specimens and consists of filter stones with a max aggregate size of 9 mm, natural sand with a fineness modulus of 2.6, and ordinary Portland cement (42.5 grade). All piles were cast from the same batch to alleviate the possibility of any bias and eliminate any variance in the material and casting process. The target concrete compressive strength is 15 MPa at 28 days. During the pile casting processing, three samples were cast and cured to evaluate the average compressive test results after 28 days.

Reinforcement steel bars were sourced from a local supplier (Ezz Steel Egypt). High tensile steel bars with a yield strength of 400 MPa were used in the longitudinal reinforcement of the reference concrete pile (PS) and the central longitudinal reinforcement of the PSGA and PSGB piles. The steel bar diameters for the longitudinal reinforcement and the central reinforcement were 8 mm and 12 mm respectively. Mild steel, with a yield strength 240 MPa, was used for the spiral stirrups in the PS and PL piles.

The GFRP bars were sourced from an international distributor (Armastek and imported by Fiber Reinforcement Industries Company) (Figure 2-a). The bars had a nominal diameter of 8 mm. The geo-synthetics geo-grids (Figure 2-b, and 2-C) were sourced from (Tensar International Corporation) and were the TX130 (GA) and TX150 (GB). Table 2 provides the mechanical properties of GFRP, and geogrid.

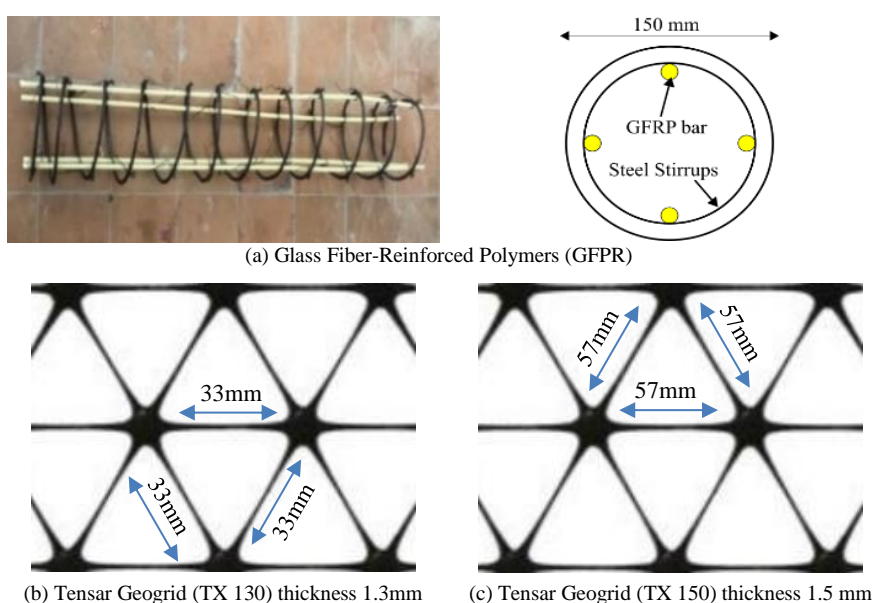


Figure 2. Typical views of the alternative pile reinforcement (a) GFRP and (b,C) Tensar geogrid

Table 2. Dimensions and Characteristic Properties of Reinforcement Materials (Armastek and imported by Fiber Reinforcement Industries Company; Sika Company; Tensar International Corporation)

Type	Dimension (mm)		Tensile strength		Modulus of elasticity (MPa)	Strain at failure (%)	Durability	
	Diameter	Thickness	(MPa)	(N/mm)			Resistance to chemical degradation (%)	Resistance to ultra-violet light and weathering (%)
L	8*	-	1100*	-	28570*	2.9*	-	-
GA	-	1.3**	-	10**	200000*	0.5*	100*	70*
GB	-	1.5**	-	11.25**	225000*	0.5*	100*	70*

* Data provided in the manufacture data sheet.

** Values from experimental measurements/results.

2.3. Test Set-Up and Instrumentations

Tests were carried out at the concrete laboratory testing facility in Benha Faculty of Engineering at the University of Benha, Egypt. and the setup is displayed in Figure 3. A rigid reaction frame was utilized to apply axial load on the hung pile specimens. Load was applied through a 1000 KN capacity hydraulic jack at the top of the pile and concrete blocks provided a base support for the test setup. To ensure that the load is distributed uniformly on the pile head, a thick steel plate was used. A load cell with a maximum capacity of 1000 KN was positioned below the hydraulic jack to measure the applied load. A strain gauge, 30 mm gauge length, was glued on the concrete surface, near the top of the pile to monitor the deformation at the top of the pile. Data was captured at a frequency of 0.5 Hz using a digital data acquisition system. A pump displacement control system was used to apply the load at a constant strain rate of 0.035 mm/min.

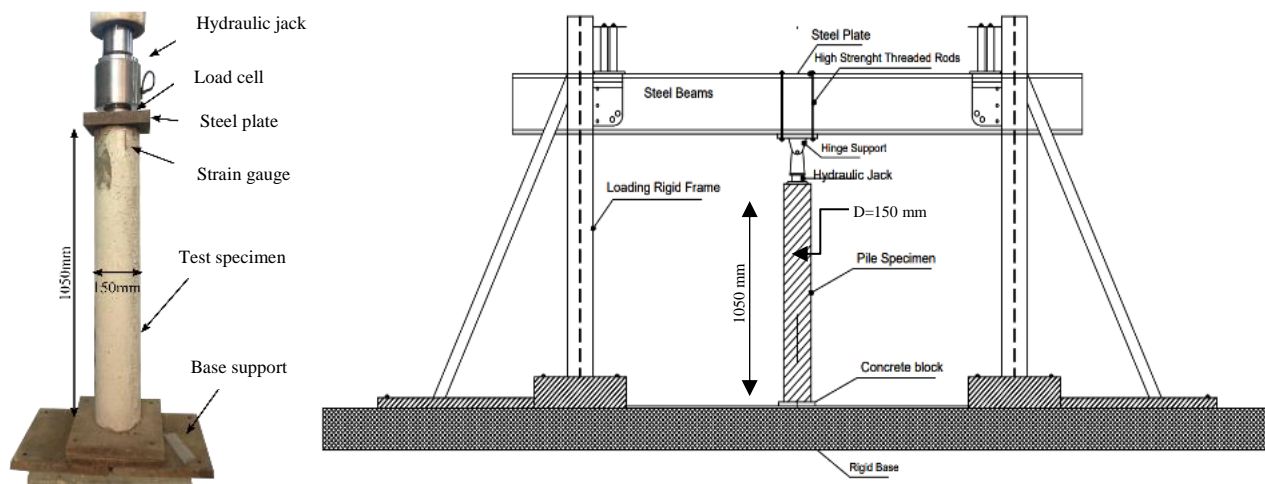


Figure 3. The test setup used in the axial capacity determination showing the various components

3. Experimental Results and Discussion

The experiments carried out aimed to monitor the pile performance, more specifically the end bearing component, under axial load using different reinforcement materials. The experimental results are shown in Table 3 which includes the ultimate axial stress, ultimate axial load, strain at ultimate stress, reinforcement weight, the ratio between the reinforcement weights, the price of reinforcement, and the change in price compared to the reference pile (PS).

Table 3. Summary of Experimental Results

Group No.	Pile Code	Ultimate Axial Load		Strain at ultimate stress *10 ⁻³ (mm/mm)	Reinforcement Weight		Reinforcement Price (USD/pile)	
		(kN)	Compared to PS %		(gm)	Compared to PS %	Year 2022	Compared to PS %
Reference	PS	222.5	-	0.555	1220	-	2.5	-
First	PL	247.3	1.11	0.731	413	34	1.8	72.5
Second	PGA	227.8	1.024	0.971	52	4.3	0.4	15.2
	PGB	226.1	1.016	0.925	80	6.6	0.7	28.5
Third	PSGA	280.8	1.254	0.722	972	79	1.5	59.6
	PSGB	243.7	1.095	0.832	1000	81	1.85	72.8

3.1. Results

The ultimate axial load and corresponding strain were recorded during each specimen test. The summary of test results is reported in Table 3. Figure 4 illustrates the evolution of the axial stress strain for all the tested groups and their pertaining samples. The reference sample (PS) recorded an ultimate stress of 12.6 MPa. In the first group, PL showed an ultimate stress of 14 MPa. For the second and third groups, the recorded ultimate stress for PGA, PGB, PSGA, and PSGB were 12.9 MPa, 12.8 MPa, 15.8 MPa, and 13.8 MPa, respectively. In terms of the percentage improvement in ultimate capacity over PS, the first group was 111% for PL. For the second and third groups, the improvement was 102.4%, 101.6%, 125.4%, and 109.6%, respectively.

The strain recorded at the ultimate stress for the PS was 0.555. The strain increased for all groups; the first group showed a strain at an ultimate stress of 0.731 for the PL samples. The second group showed a strain of 0.971 and 0.925 for the PGA and PGB piles, respectively. The third group showed a strain of 0.72 and 0.83 for the PSGA and PSGB piles, respectively.

On the other hand, the reinforcement weight decreased for all groups when compared to the PS which was 1220 gm. The first group had a weight of 413 gm. i.e., about 34% of the PS sample. In the second group, the reinforcement weights for the PGA and the PGB piles were 52 and 80 gm, i.e., about 4.3% and 6.6% of the PS sample, respectively. The third group had reinforcement weights of about 79% and 81% of the PS, at 971 gm and 1000 gm for the PSGA and PSGB specimens, respectively.

The reinforcement price decreased for all materials when compared to the PS. For the GFRP bars, the reinforcement price was about 72.5% of that of the PS sample. For the geogrid materials, the reinforcement price was 15.2 and 28.5% of the PS sample for the PGA and PGB reinforcement, respectively. For the geogrid materials with the central steel bar, the reinforcement price was 59.6 and 72.8% of that of the PS sample for the PSGA and PSGB reinforcement, respectively.

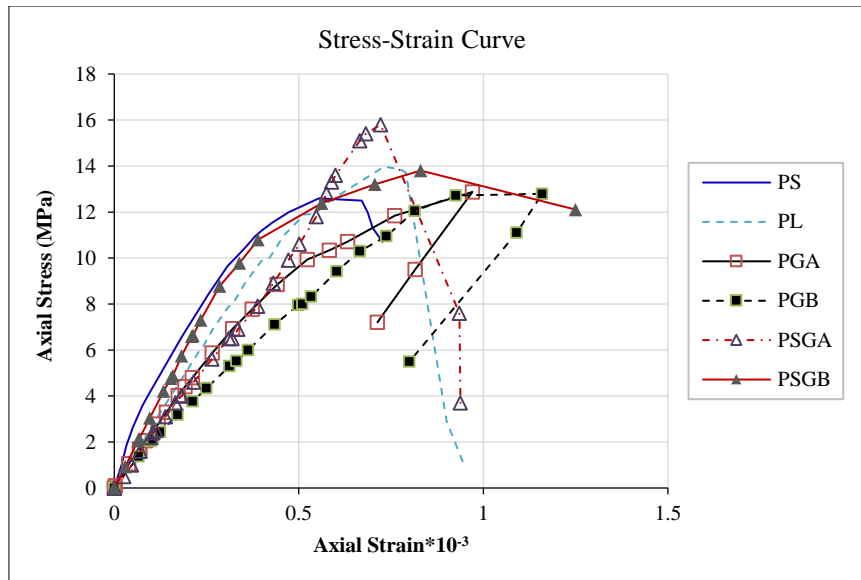


Figure 4. The evolution of the axial stress and axial strain during the pile performance experiments using different reinforcement materials

3.2. Discussion

In this section, the stress-strain behavior and modes of failure were discussed.

3.2.1. Ultimate Axial Load

The increase in the ultimate axial stress across all the groups ranged between 1.6 to 25.4% compared to PS (Figure 5). The second group showed the least performance enhancements with 1.6% and 2.4% increase with the PGA outperforming the PGB. The performance enhancement in the PGA is attributed to the flexibility of wrapping to its lower stiffness. However, it is evident that the tensile carrying capacity of the geogrid does not effectively add any load-bearing capacity to the pile capacity. On the other hand, when steel is added to the geogrid (third group), the increase in capacity changes substantially and ranges between 9.5% and 25.4% with the PSGA being the most substantial. To note is the fact that although the third group showed a substantial increase, the difference in load-carrying capacity of the PSGA and PSGB is about 15%, which is a large variation compared to the variation across the PGA and PGB samples. The ultimate capacity of the PL piles was more than the PS by 11%. Overall, it is evident that the most ideal combination that enhances the ultimate axial stresses of the pile is using a steel bar in the middle of the core alongside reinforcement with geosynthetics geogrids. More specifically, the PSGA results in an upwards of 25% increase in the load-carrying capacity with financial savings of up to 40%.

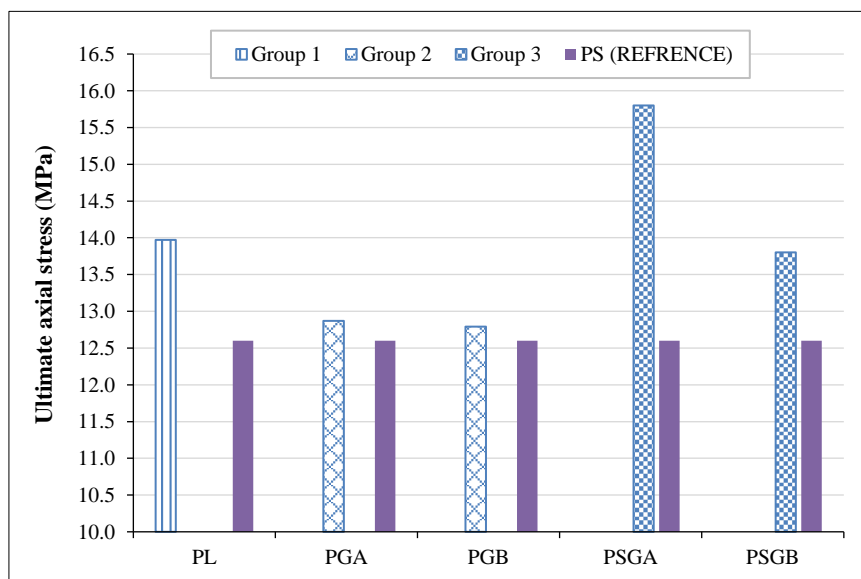


Figure 5. Comparison between specimens in terms of ultimate load

3.2.2. Strain

In terms of the sustained strain up to failure, all groups showed substantial improvement when compared to PS which was 0.55 (Figure 6). The second group showed the greatest improvement in sustaining strains ranging from 0.971 and 0.925. However, in the third group, i.e., when a steel bar is incorporated with the geogrid, the strain enhancement diminishes to about 0.731 and 0.832. Although, still larger than PS, they are about 50% lower than just using geogrids. The first group shows the least improvement of 0.702. The variation in the results can be seen through the stiffness of the reinforcement material used. When only geogrid is used, this allows for the composite material to excessively deform without taking up any damage. However, once steel reinforcement is added, this gained advantage is lost as the strain in the steel leads to rapid failure.

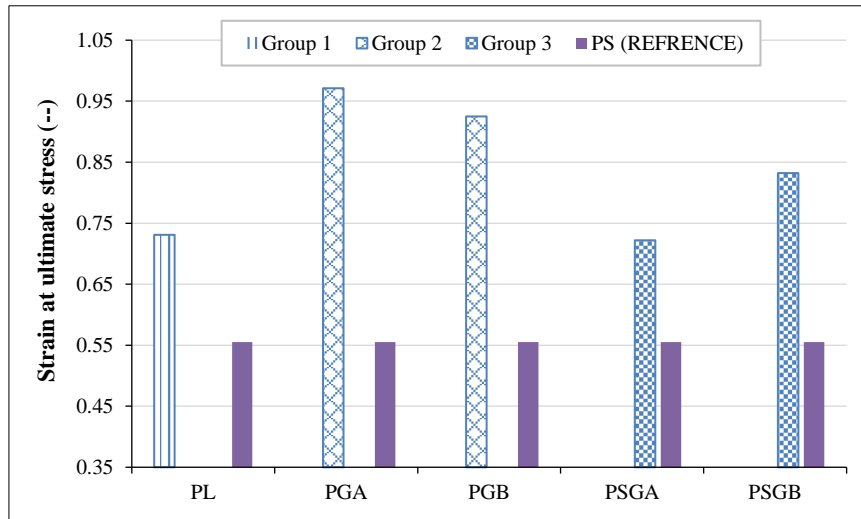


Figure 6. Comparison between specimens in terms of strain at ultimate stress

3.2.3. Modes of Failure

Post-test specimen failure modes for all groups are shown in Figure 7. All samples showed a ductile failure by compression. The evolution of the stress-strain curves reveals several post-peak observations. In all groups the post-peak stress decreases; however, in the second group, the post-peak strain decreases. In other words, the second group had a more brittle failure. The post-peak strain in the first group decreases abruptly, while in the third group, there is a prolonged period of deformation post-peak. This behaviour can be indicative of the increase in nonelastic strain which results in prolonged post-peak strain. Sample PSGB displays strain softening where there is an increase in strain post-peak. Although strain softening is a deterioration of material strength in fiber-reinforced composites and concrete, it appears to be the dominant controlling damage behavior in the geogrid with reinforcement [27].

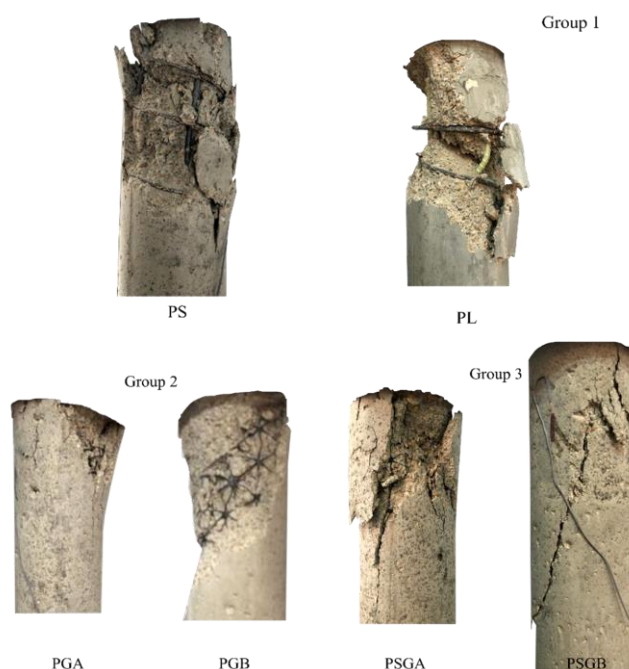


Figure 7. Failure modes for specimens

3.2.4. Cost Comparison

In all groups the reinforcement weight decreases, however, in terms of financial implications to these materials this is not so straightforward. The first group has the least financial implications, GFRP reduces the cost by about 27%. The second group has the greatest reduction in terms of financial implications reducing costs by approximately 75% to 85% when compared to PS. The third group reduces the costs by 30% to 40%. The reason for such a difference between the second and third groups is due to the incorporation of the steel reinforcement bar. Hence, it is evident that although adding a steel bar does increase efficiency it carries unfavorable financial implications and undesirable loss in overall strain of the pile.

4. Nonlinear Finite Element Analysis (NLFE)

Finite element study (NLFE), using the software ABAQUS/CAE Standard version 6.14-2 [28], was performed to replicate the normal response of reference concrete piles, and the performance of the piles within the three groups. The groups are namely PL, PGA, PGB, PSGA, and PSGB. Which are reinforced with steel bars, GFRP, and geo-synthetics geo-grids. To accurately replicate the laboratory investigation. the same material characteristics used in the laboratory investigation were adopted for the numerical simulations which include the concrete compressive strength, reinforcement bars modulus of elasticity, yield stress, steel tensile strength, FRP bars, and geosynthetics geogrids.

4.1. Geometry Model

The structural aspects of the experimental setup were replicated in ABAQUS using various types of structural elements. A three-dimensional solid element represented the concrete, while the steel bars, stirrups, and GFRP were depicted using truss elements. The geosynthetics geogrids were simulated with deformable shell planar elements, and the circular loading and support plates were modeled using rigid elements. It was assumed that a perfect bond existed between the embedded reinforcement (bars, stirrups, and geosynthetics geogrids) and the concrete. The meshing of the concrete element, reinforcement element, and plate element was done with a size of 20 mm. The model analysis followed the displacement control loading method. Figure 8 illustrates the 3D model of a typical tested pile.

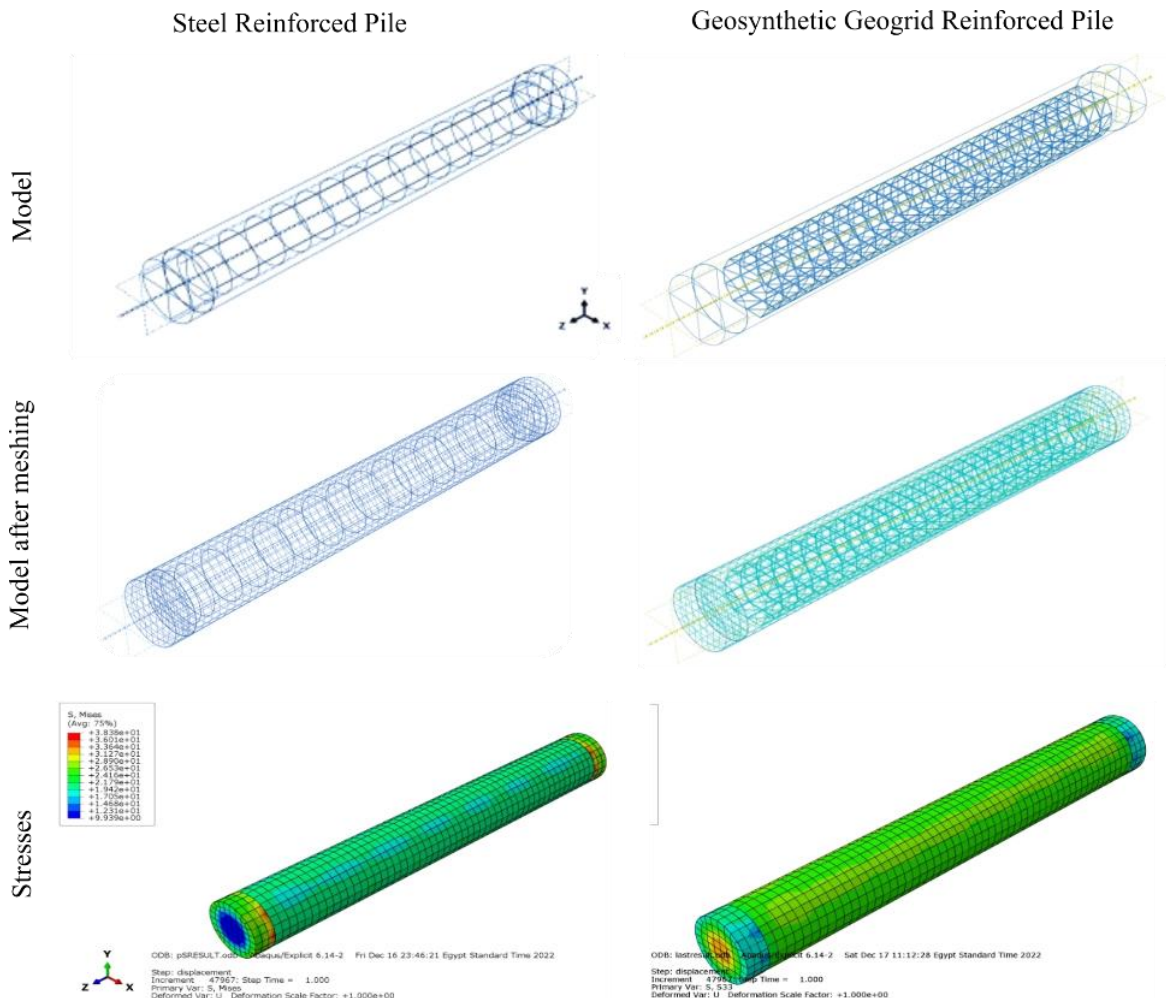


Figure 8. Typical simulation for the steel-reinforced and geogrid-reinforced pile

4.2. Concrete Behavior Modelling in Compression

The parameters for the concrete damage plasticity model (CDP) of normal concrete were established based on Zainal et al. [29], with the utilization of the following equations:

$$\sigma_c = (1 - d_c)E_0(\varepsilon_c - \varepsilon_c^{pl,h}) \tag{1}$$

$$\varepsilon_c^{in,h} = \varepsilon_c - \frac{\sigma_c}{E_0} \tag{2}$$

$$\varepsilon_c^{pl,h} = \varepsilon_c - \frac{\sigma_c}{E_0} \left(\frac{1}{1-d_c} \right) \tag{3}$$

$$\varepsilon_c^{pl,h} = \varepsilon_c^{in,h} - \frac{\sigma_c}{E_0} \left(\frac{d_c}{1-d_c} \right) \tag{4}$$

Moreover, this research employs the parabolic constitutive model formulated by Kent & Park [30] for unconfined concrete, typically represented by the equation:

$$\sigma_c = \sigma_{cu} \left[2 \left(\frac{\varepsilon_c}{\varepsilon'_c} \right) - \left(\frac{\varepsilon_c}{\varepsilon'_c} \right)^2 \right] \tag{6}$$

where, σ_c denotes the nominal compressive stress and ε_c signifies the nominal compressive strain, with the ultimate compressive strength and strain denoted as σ_{cu} and ε'_c , respectively.

The compression damage, denoted as d_c , can be calculated utilizing the subsequent expression:

$$d_c = 1 - \frac{\sigma_c}{\sigma_{cu}} \tag{7}$$

4.3. Reinforcement Modelling

The stress-strain curve depicted in Figure 9 was employed to define the characteristics of GFRP and steel bars in the idealized form. The geosynthetics geogrids were defined using the mechanical properties listed in the manufacture datasheet in Table 2-Section 2.2.

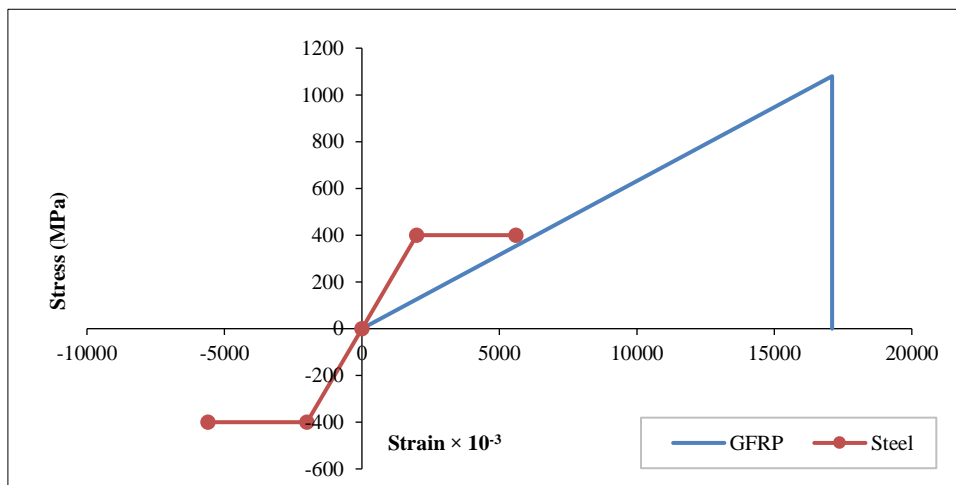


Figure 9. Constitutive models (stress-strain curve) for the various reinforcement materials, namely GFRP, and steel

To ensure that the proposed FEM approach is valid for the wide variety of pile reinforcement materials the experimental work of Zhang & Hadi [19] is utilized to verify the FEM approach. Zhang & Hadi [19] studied the behavior and axial capacity of plain previous geopolymer concrete, and their experimental results indicated a maximum axial load of 373 KN with a recorded axial strain at a maximum load of 0.0021. The FEM approach used herein resulted in an ultimate axial load of 388 KN which occurred at the strain of 0.0019. The comparison in terms of the evolution of the stress-strain curve between the experimental data and the FEM approach is depicted in Figure 10. The results showed that the variation in results does not exceed 5% for the ultimate axial load, thus implying the adequacy of the FEM approach to simulate different pile reinforcement materials.

4.4. Comparison between the Experimental and NLFE model

To validate the model, a comparison between the results of the NLFE model and experimental data was conducted. This comparison specifically examined two key aspects: the relationship between axial stress and axial strain, and the peak axial capacity.

The results of the FEM simulation were validated against the experimental results of the tested control PS specimen. Following the verification process, the FEM simulation was used to verify the performance of the various groups and materials used in the experiments, namely the PS, PL, PGA, PGB, PSGA, and PSGB. The results of simulation results showed an increase in performance in terms of the ultimate stress for PL, PGA, PGB, PSGA, and PSGB of 108.9%, 103.7%, 103%, 119.9%, and 115.2%, respectively compared to the PS specimen. The experimental evolution of the stress strain was captured with good accuracy in the FEM simulation as presented in Figure 11. This indicates the robustness of the methodology and its ability to reflect the effect of different reinforcement materials on the axial stress of the piles.

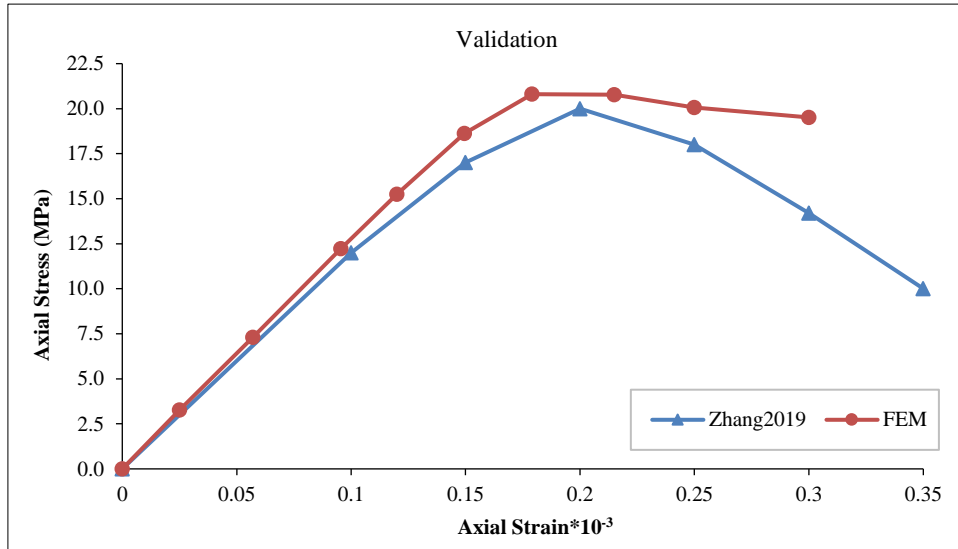
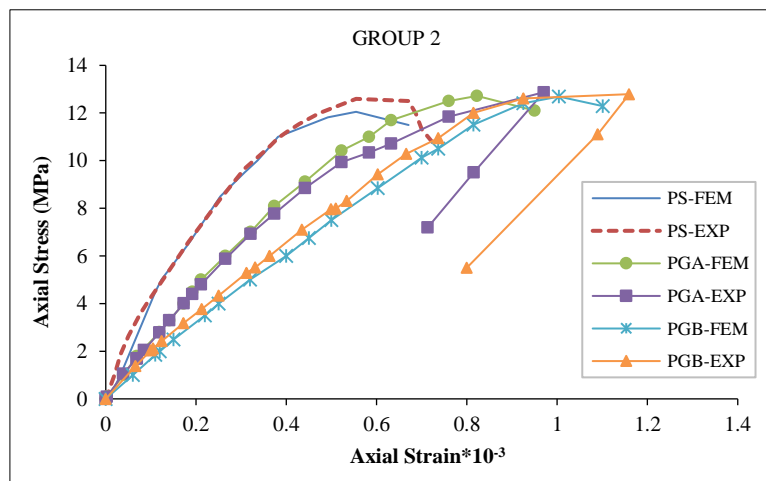
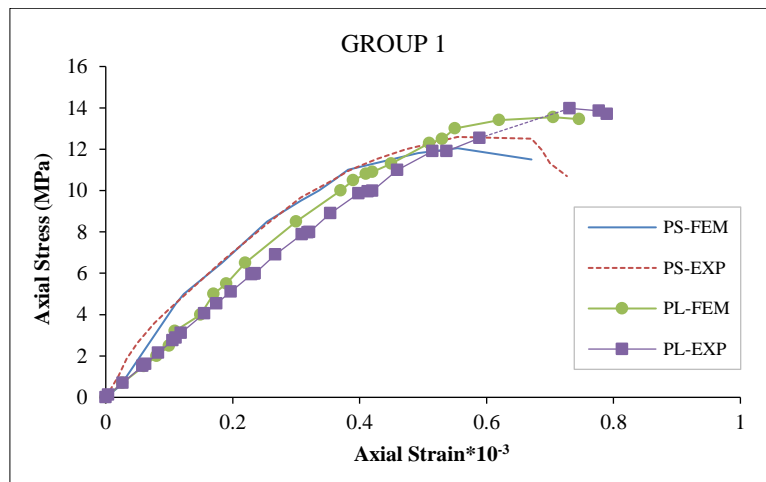


Figure 10. Comparison between (Zhang & Hadi (2019) [19]) and FEM Stress-strain curve



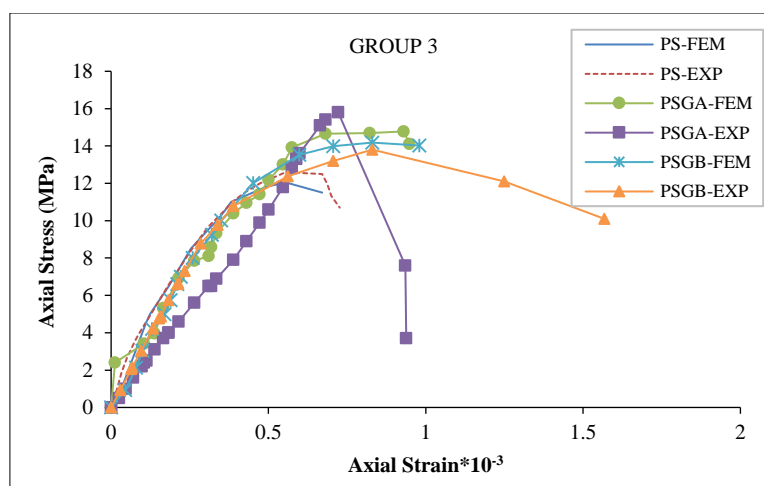


Figure 11. Stress–Strain relationship for experimental and FEM

The comparison of the ultimate stress from the experimental results (P_{EXP}) and FEM simulation (P_{FEM}) is shown in Table 4.

Table 4. Comparison of Experimental and FEM Results

Pile code	$P_{EXP}(kN)$	$P_{FEM}(kN)$	P_{EXP}/P_{FE}
PS	222.6	217.6	1.023
PL	247.3	236.9	1.04
PGA	227.8	225.7	1.01
PGB	226.1	224.2	1.01
PSGA	280.8	260.99	1.08
PSGB	243.7	250.6	0.97
<i>Average</i>			<i>1.022</i>

Since the methodology has proven adequate in representing the pile reinforced with various materials, a 3D nonlinear finite element simulation is conducted to simulate pile-soil interaction (Figure 12). This step is conducted to validate that the absence of restraint in the experimental setup has minimal impacts on the performance of the pile as well as its load-bearing capacity. This is achieved by modeling a pile surrounded by soft clay soil and resting on crushed rock soil. A 3D deformable solid part was used to model the soil, concrete pile, and top plate. A 3D deformable wire element was used to model the steel longitudinal bars and stirrups. The reinforcement was modeled as an embedded element within the concrete element. A linear elastic stress-strain curve was specified for the steel bars. The full length of the concrete pile specimen was modeled and assumed to be completely embedded in the modeled soil. A ring plate was modeled to accommodate the geometry at the loading. The pile was configured as an explicit body. The interaction between the soil and the pile is modeled as a surface-to-surface tie contact. For the boundary condition, the soil was allowed to deform in the direction of the applied load similar to in-situ conditions. The properties of soil and crushed rock are defined in Table 5.

Table 5. Soil Properties

Type of soil	Modulus of elasticity (MPa)	Poisson’s ratio (-)	Friction angle (°)	Cohesion (kPa)
Crushed rocks	100	0.05	40	0

The result obtained from the FEM simulation for the pile-soil analytical model (with simulating the soil) was verified against the result obtained from the FEM simulation for the pile analytical model (without simulating soil). The ultimate axial load for the pile soil and the pile model were 224.4 KN and 217.6 KN, respectively. The results showed good convergence with and without simulating the soil in the analytical model by 3.13%. Hence, it can be concluded that the effect of the soil, within the constraints of the numerical parameters and boundary conditions, was negligible in the FEM and thus the proposed experimental setup and results are deemed acceptable.

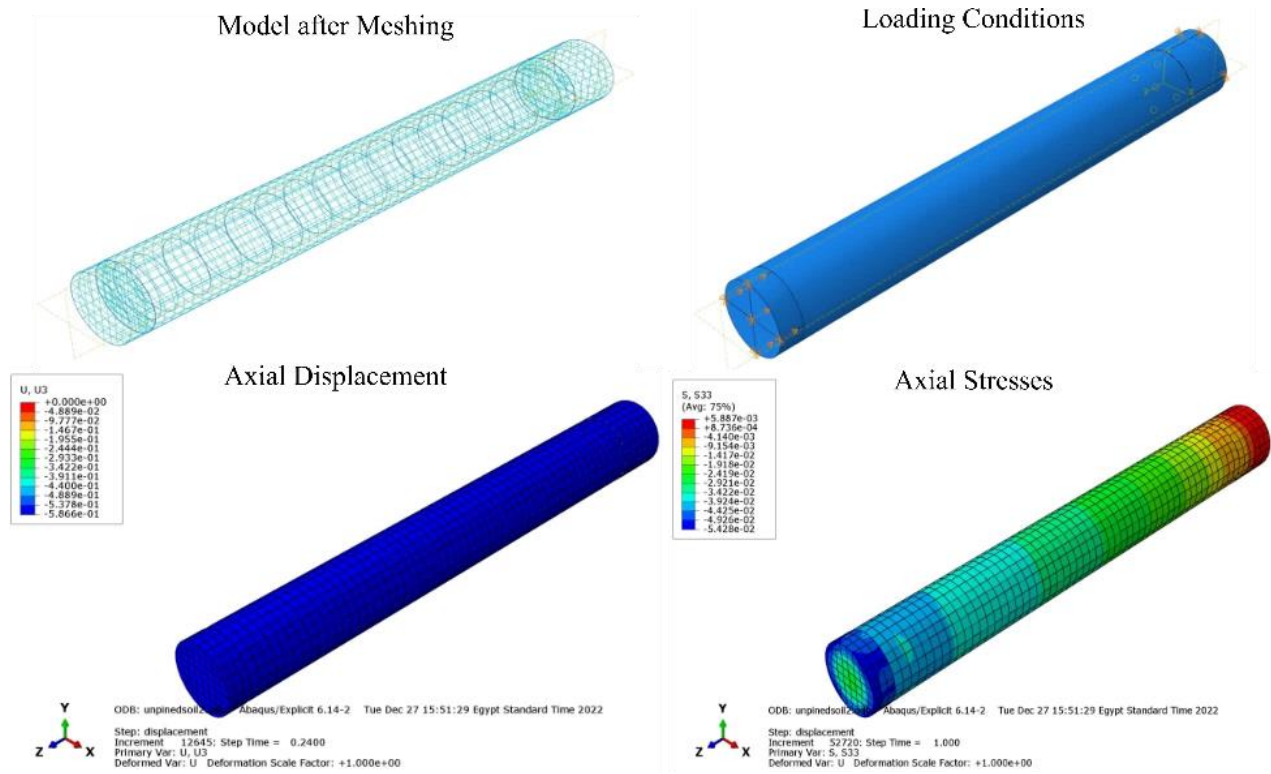


Figure 12. Simulation of reinforcement concrete pile rested on crushed rocks soil

5. Analytical Calculations

All specimens were tested for failure under axial load. The predicted ultimate loads (P_u) of the control specimen can be estimated by using Equation 7 in accordance with the ACI 318M-11 [26].

$$P_u = 0.85 \times f_c' \times (A_c - A_s) + \mathcal{E}_y \times E_s \times A_s \tag{7}$$

where f_c' is the concrete cylinder compressive strength at 28 days, A_c is the area of concrete, E_s is the modulus of elasticity of the reinforcement material used, \mathcal{E}_y is the strain of the reinforcement material, and A_s is the area of the reinforcement bars.

As shown from the above, the ACI 440.1R-15 [31] and the local guidelines in the Egyptian Code of Practice 203-2020 [32] lack calculations of the ultimate axial load of piles reinforced with GFRP, geosynthetics geogrids, and/or a combination thereof with embedded steel. Hence, based on the experimental results above and the FEM modeling, the design equation (Equation 8) is suggested for the evaluation of the ultimate load capacity of specimens reinforced by GFRP or geosynthetics geogrids:

$$P_u = 0.85 \times f_c' \times (A_c - (A_G + A_{sb})) + \phi_G \times \mathcal{E}_y \times E_G \times A_G + \phi_b \times \mathcal{E}_y \times E_{sb} \times A_{sb} \tag{8}$$

where f_c' is the concrete cylinder compressive strength at 28 days, A_c is the area of concrete, E_G is the modulus of elasticity of geosynthetics geogrids, A_G is the effective area of geosynthetics geogrids, ϕ_G is the reduction factor of the geosynthetics geogrids, E_{sb} is the modulus of elasticity of the reinforcement bars used, \mathcal{E}_y is the strain of the material, A_{sb} is the area of reinforcement bars used, and ϕ_b is the reduction factor of the reinforcement bars used. The ultimate axial load for composite piles reinforced with steel was predicted using the analytical model modified by Hadhood et al. [33]. The new approach proposes the reduction factor ϕ_G that is dependent on the geosynthetics geogrids material and a reduction factor ϕ_b dependent on the material of the reinforcement bar used in the core. A Comparison is held between the ultimate peak capacity of the experimental (P_{EXP}), FEM (P_{FE}), and predicted results using Equation (8) (P_{TH}) exhibit great convergence, in the order of ± 20 kN, as detailed in Figure 13, and Table 6.

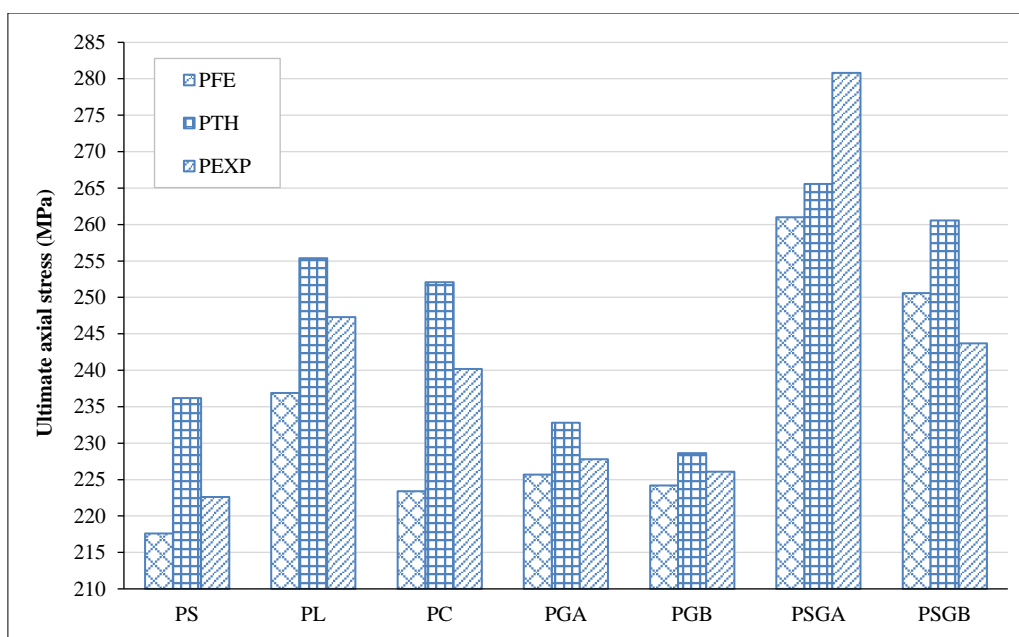


Figure 13. Comparison between experimental, FEM, and calculated results

Table 6. Comparison of Experimental, FEM, and Theoretical Results

Pile code	ϕ_b	ϕ_G	Ultimate Capacity (kN)			P_{TH}/P_{EXP}
			P_{FEM}	P_{TH}	P_{EXP}	
PS	1.00	-	217.60	236.20	222.6	1.06
PL	0.65	-	236.90	255.40	247.3	1.03
PGA	-	0.25	225.70	232.80	227.8	1.02
PGB	-	0.20	224.20	228.61	226.1	1.01
PSGA	1.00	0.25	260.99	265.57	280.8	0.95
PSGB	1.00	0.20	250.60	260.58	243.7	1.07

6. Conclusions

The work presented herein included a set of experimental tests to examine the ultimate load capacity of piles reinforced with different commercially available materials. The reinforcing materials ranged from glass fiber bars to geosynthetic grids that were additionally reinforced with a steel bar. The results of the experiments were used to verify the nonlinear approach adopted in the FEM and further evaluate and predict the performance of the various materials. Additionally, a theoretical equation has been suggested showing great convergence with the experimental results. The following conclusions are also brought forward:

- Using GFRP bars or geosynthetics geogrids boosting the ultimate axial stress of the pile compared to PS, the ultimate axial stress was increased by 11% for specimens reinforced with FRP bars, 1.6-2.4% for specimens reinforced with geosynthetics geogrids, and by 9.5-25.4% for specimens reinforced with geosynthetics geogrids and middle core of steel bar.
- Using GFRP bars or geosynthetics geogrids boosting the strain of the pile compared to PS, the strain was increased to 0.92 & 0.97 for specimens reinforced with PGA & PGP respectively. And 0.55 for PS.
- Geosynthetics geogrids with a middle core of steel bar response better in terms of ultimate capacity when compared to geosynthetics geogrids only.
- The weight for all reinforced specimens was decreased effectively between 4.3% to 81% when compared to PS.
- The cost of the reinforcement for all the pile specimens reinforced by GFRP bars or geosynthetics geogrids was reduced effectively from 25% to 85%.
- A ductile response was captured in all specimens reinforced by geosynthetics geogrids or steel bars.
- Nonlinear finite element analysis has been verified and achieved a great convergence against the experimental results.
- A proposed formula to account for the impact of geosynthetic geogrid material with additional reinforcement bars on the pile capacity.

7. Declarations

7.1. Author Contributions

Conceptualization, E.A.E. and M.I.B.; methodology, E.A.E. and M.I.B.; software, M.I.B.; data curation, M.I.B.; writing—original draft preparation, M.I.B.; writing—review and editing, M.A.; visualization, M.I.B. and M.A.; supervision, M.A.; funding acquisition, M.R. All authors have read and agreed to the published version of the manuscript.

7.2. Data Availability Statement

The data presented in this study are available in the article.

7.3. Funding

The authors received no financial support for the research, authorship, and/or publication of this article.

7.4. Conflicts of Interest

The authors declare no conflict of interest.

8. References

- [1] Iskander, M. G., Hanna, S., & Stachula, A. (2001). Driveability of FRP Composite Piling. *Journal of Geotechnical and Geoenvironmental Engineering*, 127(2), 169–176. doi:10.1061/(asce)1090-0241(2001)127:2(169).
- [2] Iskander, M. G., & Stachula, A. (2002). Wave Equation Analyses of Fiber-Reinforced Polymer Composite Piling. *Journal of Composites for Construction*, 6(2), 88–96. doi:10.1061/(asce)1090-0268(2002)6:2(88).
- [3] Abdel-Karim, A. H., Khalil, G. I., Ewis, A. E., & Makhlof, M. H. (2023). Impact of developed hybrid polypropylene fiber inclusion on the flexural performance of concrete beams reinforced with innovative hybrid bars. *Construction and Building Materials*, 409(134113). doi:10.1016/j.conbuildmat.2023.134113.
- [4] Sen, R., & Mullins, G. (2007). Application of FRP composites for underwater piles repair. *Composites Part B: Engineering*, 38(5–6), 751–758. doi:10.1016/j.compositesb.2006.07.011.
- [5] Zyka, K., & Mohajerani, A. (2016). Composite piles: A review. *Construction and Building Materials*, 107, 394–410. doi:10.1016/j.conbuildmat.2016.01.013.
- [6] Benmokrane, B., & Ali, A. H. (2019). Review and assessment of various theories for modeling durability of GFRP reinforcement for concrete structures. *Advances in Engineering Materials, Structures and Systems: Innovations, Mechanics and Applications*, CRC Press, Boca Raton, United States. doi:10.1201/9780429426506-273.
- [7] Ding, L., Seliem, H. M., Rizkalla, S. H., Wu, G., & Wu, Z. (2011). Behavior of concrete piles confined with CFRP grid. *ACI Special Publication*, 1(275), 189–205.
- [8] Fam, A., Pando, M., Filz, G., & Rizkalla, S. (2003). Precast piles for route 40 bridge in Virginia using concrete filled FRP tubes. *PCI Journal*, 48(3), 32–45. doi:10.15554/pcij.05012003.32.45.
- [9] Giraldo, J., & Rayhani, M. T. (2013). Influence of Fiber-Reinforced Polymers on Pile-Soil Interface Strength in Clays. *Advances in Civil Engineering Materials*, 2(1), 534–550. doi:10.1520/ACEM20120043.
- [10] Giraldo, J., & Rayhani, M. T. (2014). Load transfer of hollow Fiber-Reinforced Polymer (FRP) piles in soft clay. *Transportation Geotechnics*, 1(2), 63–73. doi:10.1016/j.trgeo.2014.03.002.
- [11] Gupta, P. K., & Verma, V. K. (2016). Study of concrete-filled unplasticized poly-vinyl chloride tubes in marine environment. *Proceedings of the Institution of Mechanical Engineers Part M: Journal of Engineering for the Maritime Environment*, 230(2), 229–240. doi:10.1177/1475090214560448.
- [12] Hadi, M. N. S., & Youssef, J. (2016). Experimental Investigation of GFRP-Reinforced and GFRP-Encased Square Concrete Specimens under Axial and Eccentric Load, and Four-Point Bending Test. *Journal of Composites for Construction*, 20(5), 04013017–1. doi:10.1061/(asce)cc.1943-5614.0000675.
- [13] Iskander, M. G., & Hassan, M. (1998). State of the Practice Review in FRP Composite Piling. *Journal of Composites for Construction*, 2(3), 116–120. doi:10.1061/(asce)1090-0268(1998)2:3(116).
- [14] Suleiman, M. T., Ni, L., & Raich, A. (2014). Development of Pervious Concrete Pile Ground-Improvement Alternative and Behavior under Vertical Loading. *Journal of Geotechnical and Geoenvironmental Engineering*, 140(7), 04014035. doi:10.1061/(asce)gt.1943-5606.0001135.
- [15] Wang, W., Sheikh, M. N., & Hadi, M. N. S. (2015). Axial compressive behaviour of concrete confined with polymer grid. *Materials and Structures*, 49(9), 3893–3908. doi:10.1617/s11527-015-0761-9.

- [16] Giraldo Velez, J. D. (2013). Experimental study of Hollow Fibre Reinforced Polymer Piles in soft clay. PhD Thesis, Carleton University, Ottawa, Canada.
- [17] Guades, E., Aravinthan, T., Islam, M., & Manalo, A. (2012). A review on the driving performance of FRP composite piles. *Composite Structures*, 94(6), 1932–1942. doi:10.1016/j.compstruct.2012.02.004.
- [18] Pando, A. M., Ealy, C.D., Flitz, M. G., Lesko, J. J., & Hoppe, E.J. (2006). A Laboratory and Field Study of Composite Piles for Bridge Substructures. FHWA-HRT04-043, Federal Highway Administration, Washington, United States.
- [19] Zhang, H., & Hadi, M. N. S. (2019). Geogrid-confined pervious geopolymer concrete piles with FRP-PVC-confined concrete core: Concept and behaviour. *Construction and Building Materials*, 211, 12–25. doi:10.1016/j.conbuildmat.2019.03.231.
- [20] AlAjarmeh, O. S., Manalo, A. C., Benmokrane, B., Karunasena, W., & Mendis, P. (2019). Axial performance of hollow concrete columns reinforced with GFRP composite bars with different reinforcement ratios. *Composite Structures*, 213(2), 153–164. doi:10.1016/j.compstruct.2019.01.096.
- [21] Pham, T. A., Tran, Q.-A., Villard, P., & Dias, D. (2023). Numerical Analysis of Geosynthetic-Reinforced and Pile-Supported Embankments Considering Integrated Soil-Structure Interactions. *Geotechnical and Geological Engineering*, 42(1), 185–206. doi:10.1007/s10706-023-02564-9.
- [22] Alsirawan, R., Alnmr, A., & Koch, E. (2023). Experimental and Numerical Investigation of Geosynthetic-Reinforced Pile-Supported Embankments for Loose Sandy Soils. *Buildings*, 13(9). doi:10.3390/buildings13092179.
- [23] Alsirawan, R., Koch, E., & Alnmr, A. (2023). Proposed Method for the Design of Geosynthetic-Reinforced Pile-Supported (GRPS) Embankments. *Sustainability*, 15(7), 6196. doi:10.3390/su15076196.
- [24] Alnmr, A., & Alsirawan, R. (2024). Numerical Study of the Effect of the Shape and Area of Shallow Foundations on the Bearing Capacity of Sandy Soils. *Acta Polytechnica Hungarica*, 21(1), 103–120. doi:10.12700/APH.21.1.2024.1.7.
- [25] Pham, T. A. (2020). Analysis of geosynthetic-reinforced pile-supported embankment with soil-structure interaction models. *Computers and Geotechnics*, 121, 103438. doi:10.1016/j.compgeo.2020.103438.
- [26] ACI 318M-11. (2011). Building Code Requirements for Structural Concrete and Commentary. American Concrete Institute, Michigan, United States.
- [27] Vignjevic, R., Djordjevic, N., Vuyst, T. De, & Gemkow, S. (2018). Modelling of strain softening materials based on equivalent damage force. *Computer Methods in Applied Mechanics and Engineering*, 335(12), 52–68. doi:10.1016/j.cma.2018.01.049.
- [28] ABAQUS. (2013). Abaqus Documentation User's Guide. Dassault Systèmes, Vélizy-Villacoublay, France.
- [29] Zainal, S. M. I. S., Hejazi, F., Aziz, F. N. A. Abd., & Jaafar, M. S. (2020). Constitutive Modeling of New Synthetic Hybrid Fibers Reinforced Concrete from Experimental Testing in Uniaxial Compression and Tension. *Crystals*, 10(10), 885. doi:10.3390/cryst10100885.
- [30] Kent, D. C., & Park, R. (1971). Flexural Members with Confined Concrete. *Journal of the Structural Division*, 97(7), 1969–1990. doi:10.1061/jsdeag.0002957.
- [31] ACI 440.1R-15. (2015). Guide for the Design and Construction of Concrete Reinforced with Fiber Reinforced Polymer (FRP) Bars. American Concrete Institute (ACI), Michigan, United States.
- [32] ECP-201. (2012) Egyptian Code of Practice for Calculation of Loads and Forces in Structures and Buildings. National Housing and Building Research Center, Cairo, Egypt.
- [33] Hadhood, A., Mohamed, H. M., Ghrib, F., & Benmokrane, B. (2017). Efficiency of glass-fiber reinforced-polymer (GFRP) discrete hoops and bars in concrete columns under combined axial and flexural loads. *Composites Part B: Engineering*, 114(5), 223–236. doi:10.1016/j.compositesb.2017.01.063.